Analytical and numerical simulation of Ring Cusp Discharge Chamber

IEPC-2019-905

Presented at the 36th International Electric Propulsion Conference
University of Vienna • Vienna, Austria
September15-20, 2019

F. Cannat[1], F. Guarducci[2]and S. B. Gabriel[3]
Mars Space Ltd, Southampton, SO14 5FF, UK

Abstract: In the recent years Mars Space Limited (MSL) has been involved in the development of a ring cusp discharge chamber for ion thrusters. Analytical and numerical tools have been developed internally in order to help the sizing and optimization of future developments and evolutions of ring cusp thrusters. Experimental data from several ring cusp discharge chamber configurations have been collected in the MSL laboratory, allowing a comparison between the developed analytical and numerical tools and experimental results. The results of this comparison are presented in this paper. Discrepancies between model and experiments are discussed and possible model improvements are proposed.

Nomenclature

γ = coefficient of the recombined ion at the accel grid leaving the DC
I_{acc} = ion current collected by the accel grid
I_B = ion beam
I_{scr} = ion current collected by the screen grid
I_{tot} = ion current reached the ion optics
T_{dc} = ion optics transparency
Q_{in} = injected mass flow rate
q = elementary charge
η_p = mass utilization efficiency
u_0 = neutral velocity
A_g = grid extraction area
T_s = geometrical grid transparency
η_c = clausing factor
$\dot{m}_{ing}$ = ingested mass flow rate
$\dot{m}_{main}$ = injected mass flow rate in main
$\dot{m}_{cath}$ = injected mass flow rate in cathode
I_D = discharge current
I_e = primary current
u_B = Bohm velocity
n = Plasma density
T_{eV} = Electron temperature
I_p = ion production

[1]Electric Propulsion research engineer, Mars Space Limited, felix.cannat@mars-space.co.uk
[2] Head of modelling, Mars Space Limited, francesco.guarducci@mars-space.co.uk
[3] Director, Mars Space Limited, stephen.gabriel@mars-space.co.uk

I_{ia}	=	ion collected at the anode
P_{out}	=	power losses in the DC
I_L	=	primary current collected at the anode
V_k	=	primary energy
ε_{iz}	=	energy ionization
ε_{ex}	=	energy excitation
I^*	=	equivalent current of excited neutral
V_p	=	plasma potential
ϕ	=	sheath drop potential
I_a	=	secondaries current collected at the anode
ε_b	=	ion production cost
V_D	=	discharge potential

Superscript
^ designates without beam extraction

I. Introduction

In recent years a modular Ring Cusp Discharge Chamber (RCDC) with an inner diameter of approx. 30 cm has been developed, tested and characterized, with numbers of operating conditions and magnetic field configuration, in the Mars Space Ltd propulsion laboratory within the frame of an ESA funded project [1] [2]. The RCDC has been designed to have an ion production cost as low as 160 eV/ion for extracted beam currents in the range of 1 to 4 A. The RCDC was tested without beam extraction and using the technique described by Brophy [3] to predict the thruster performances. The highest simulated ion beam during the test campaign is 3.9A for with an ion production cost of 150 eV/ion. In addition, plasma measurements with Langmuir probe (LP) were taken to characterise plasma properties at the grid exit and optimize the flatness of the ion flux reaching the grid by testing different magnetic field topologies.

The technique of operating the Discharge Chamber (DC) without beam extraction, proposed by Brophy [3], have been mainly used during the last two decades to characterize and optimise DC in laboratories [4] [5] [6]. The main advantage of using this technique lies in the simplicity of the experimental setup which doesn't need high voltage to bias grid and gives more flexibility in DC test campaign. When the thruster is operating without beam extraction, i.e. without the high voltage bias on the grids, the ion optics transparency is reduced dramatically, changing the discharge equilibrium. The ions striking the grids recombine as neutral atoms and a fraction of these re-enters in the DC, while others leave it. The fraction which re-enters in the DC increases the neutral density in the discharge changes the overall equilibrium between species to compare with the beam extraction. In addition the collected current at the ion optics is higher than with beam extraction which changes the current balance in the DC.

In parallel, two main codes were developed at Mars Space Ltd as design and optimization tools to predict and improve the performance of the RCDC: an analytical 0D model and a numerical 2D axisymmetric code based with the work proposed by Katz and Goebel book [7] and Wirz thesis [8]. These models have been written for ring cusp ion thruster with beam extraction. To compare data from our test campaign, both models have been to take into account the discharge equilibrium which occurs when operating the discharge chamber without beam extraction.

This paper describes the adaptation from the original codes, as well as the tuning process and validation of the codes against the experimental data from the RCDC characterization test campaign.

II. Equilibrium in Ring Cusp Discharge Chamber without beam extraction

The classic model to solve the equilibrium in a Ring Cusp Ion thruster is described in [7]. This model has been written to balance ring cusp discharge chamber at the steady-state with beam extraction. To describe the equilibrium three conservation laws are used: mass continuity, currents conservation, and power conservation. In order to take into account the new equilibrium due to the absence of an extracted beam, each of these relations should be revisited to model the RCDC without beam extraction.

A. Mass continuity

The mass continuity links the injected mass and the mass utilization efficiency in the discharge chamber. The relation in the classical model is given by

$$Q_{in}\left(1-\eta_p\right)=\frac{1}{4}n_0 u_0 A_g T_s \eta_c$$

where Q_{in} is the injected particle flow rate, η_p is the mass utilisation efficiency, n_0 is neutral density, u_0 is neutral velocity, $A_g$is the active surface beam, T_s is geometrical grid transparency and η_c the clausing factor, the mass utilisation η_p is defined as

$$\eta_p=\frac{I_b}{qQ_{in}}$$

where I_b is the ion beam current. In the case without beam extraction, the grid transparency drops and a smaller fraction current reaching the grid is extracted. The mass utilization efficiency is defined as

$$\hat{\eta}_p=\frac{\widehat{T_{dc}}I_{tot}}{q\widehat{Q_{in}}}=\frac{\widehat{I_b}}{q\widehat{Q_{in}}}$$

where the hat is used as quantities for the case without beam extraction, $\widehat{T_{dc}}$ is the ion grid transparency and I_{tot} is the ion current reaching the grid. The grids transparency to ions without beam extraction is defined as

$$\widehat{T_{dc}}=\frac{\widehat{I_{res}}+\hat{I}_{acc}\gamma}{I_{tot}}\approx 23\%$$

where $\widehat{I_{res}}$ is the residual ion beam, $\hat{I}_{acc}\gamma$ is the fraction of the ion flux recombining on the accel grid that leaves effectively the DC, where γ is defined at 0.55 [3]. On the other hand, the fraction which re-enters inside the thruster increases the neutral density in the discharge chamber, consequently the mass flow rate injected inside the discharge chamber should be reduced in proportion to simulate the same neutral density inside the DC.

$$n_0=\frac{4Q_{in}\left(1-\eta_p\right)}{u_0 A_g T_s \eta_c}=\widehat{n_0}=\frac{4\widehat{Q_{in}}\left(1-\hat{\eta}_p\right)}{u_0 A_g T_s \eta_c}$$

B. Current conservation

In the case of operation with beam extraction, the ion flux reaching the grid is divided between the current screen grid and the ion beam and the accel grid current is negligible. The current conservation from the cathode point of view and the ion production equations are defined as

$$I_e=I_d-I_s-I_k$$

$$I_p=I_{ia}+I_s+I_b$$

where I_e is the primary current injected through the cathode, I_d is the discharge current, I_s is the ion current at the screen grid, I_k is the ion current at the keeper, I_p is the ion production in the discharge and I_{ia} is the ion current collected at the anode. In the case without extracted beam, the ion flux reaching the grid is collected on the grids while the residual ion beam is negligible, the new current conservation from the cathode point of view and the ion production equations become

$$\widehat{I_e}=\widehat{I_d}-I_{tot}-\widehat{I_k}$$

$$\widehat{I_p}=\widehat{I_{ia}}+I_{tot}$$

where the total ion flux reaching the grids I_{tot} is defined as

$$I_{tot} = \frac{1}{2} q\hat{n}\widehat{u_B}A_g$$

where n is the plasma density and u_B the ion Bohm velocity

C. Power conservation

The power in the discharge chamber is balanced between the current emitted from the hollow cathode time its energy gain in DC. This power is transferred from the primaries to ionization, excitation, and Maxwellian electrons, and leaving the DC as ion and electron current. In the case of the DC with beam extraction the relation is written as

$$I_e V_k = I_p \varepsilon_{iz} + I^* \varepsilon_{ex} + (I_s + I_k)(V_d + V_p + \phi) + (I_{ia} + I_b)(V_p + \phi) + I_a(2T_{eV} + \phi) + I_L V_k$$

where V_k is the primary energy gain in DC, ε_{iz} is the energy used per ionization collision, ε_{ex} is the energy used per excitation collision, I^* is the produced excited neutral, V_d is the discharge voltage, V_p is the plasma potential, ϕ is the potential drop at the cusps, I_a is the secondaries collection at the anode, electron, I_L is the primary current collection at the anode and T_{eV} is the electron temperature. In the case of the DC without beam extraction, a smallest fraction of ion leaves the DC as beam and more current is collected on the grid

$$\widehat{I_e}\widehat{V_k} = \widehat{I_p}\varepsilon_{iz} + \widehat{I^*}\varepsilon_{ex} + (I_{tot} + \widehat{I_k})(\widehat{V_d} + \widehat{V_p} + \hat{\phi}) + (\widehat{I_{res}} + \widehat{I_{ia}})(\widehat{V_p} + \hat{\phi}) + \widehat{I_a}(2\widehat{T_{eV}} + \hat{\phi}) + \widehat{I_L}\widehat{V_k}$$

III. Comparison of the 0D model with and without beam extraction

Two analytical 0D models have been written, one without beam and one with beam extraction to compare and validate equations proposed previously. To compare both models, these should respect three criteria of similarity.

- The neutral density should be equal
- The ion flux reaching the grid should be equal
- The discharge chamber should simulate the same discharge curves

The technique described by Brophy [3] allows estimating which equivalent performances and operating conditions the discharge chamber tested without beam would operate if high voltage is applied to the grid, as ion beam, mass utilisation efficiency, mass flow rate and the ion production cost.

$$I_B = T_{dc} I_{tot}$$

$$\eta_p = \frac{I_B}{q\widehat{Q_{in}} + I_B\left(1 - \frac{\widehat{T_{dc}}}{T_{dc}}\right)}$$

$$Q_{in} = \frac{\widehat{Q_{in}}}{1 - \eta_p\left(1 - \frac{\widehat{T_{dc}}}{T_{dc}}\right)}$$

$$\varepsilon_b = \frac{(\widehat{I_D} - I_B)\widehat{V_D}}{I_B} \Leftrightarrow \frac{I_D V_D}{I_B}$$

By running the 0D model without beam extraction and using they predicted operating conditions and performances in the 0D model with beam performances, the balance characteristics can be compared.

A. Test case comparison of the 0D model with and without beam extraction

The 0D model without beam extraction is set with a test case base on a ring cusp discharge chamber and operating conditions used during the test campaign. This model is run by sweeping the mass flow rate between 15 and 30 SCCM, for a constant discharge current of 23 A and an ion beam of 3 A. Outputs of the 0D model without beam extraction such as the simulated mass utilization efficiency, mass flow rate and ion production cost are then used as input in the 0D model with beam extraction to compare balance characteristics. In the model with beam extraction, instead of fixing the discharge current as inputs, the ion cost is fixed and the discharge current and voltage are solved. In our test case, the outputs coming from the model without beam and given to the 0D model with beam extraction provide a simulated mass utilization efficiency varying between 67 % and 92 %, a total mass flow rate between 44.5 SCCM and 61 SCCM and a simulated ion cost between 171 eV/ion and 188 eV/ion.

Figure III-1 shows the neutral density for both models, for the ranges of mass flow rates used in the different models, the neutral densities solved are equal in respect of the equivalent mass flow rate used for the model with beam extraction.

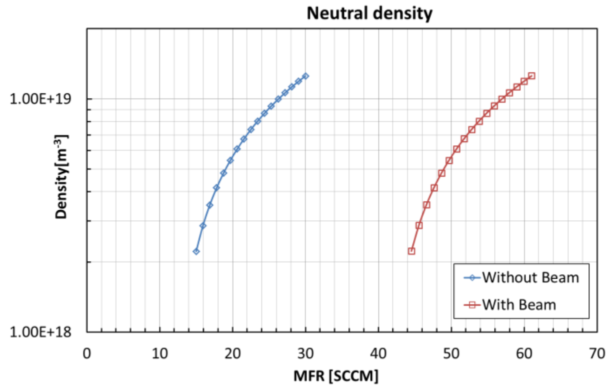

Figure III-1Theoretical similarity comparison – Neutral density

Figure III-2 compare electrical discharge characteristics with and without beam extraction. For what concerns the discharge current, it should be noted that first, the current needed to obtain the same discharge curve is close to the discharge current without beam. Secondly, the discharge voltage needed to sustain the balance in the case with beam extraction is much lower than the case without beam extraction.

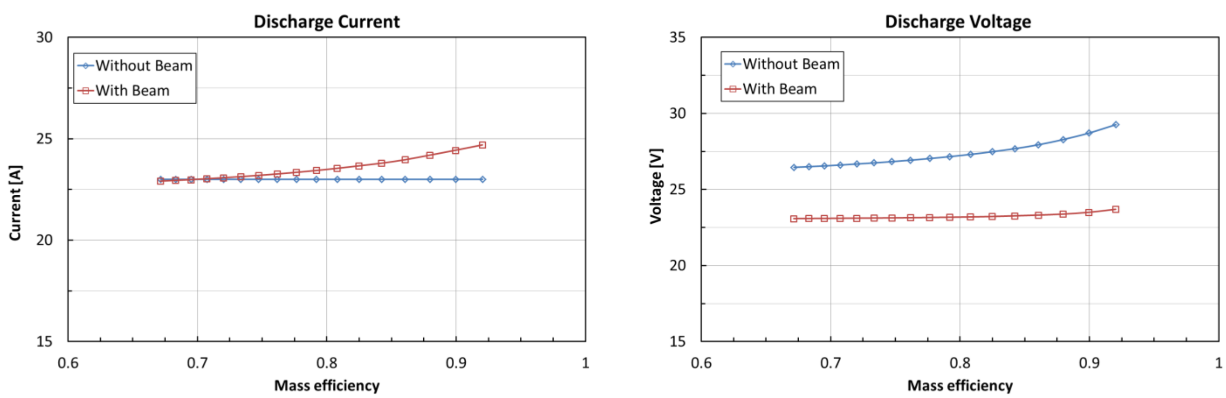

Figure III-2 Electrical discharge characteristics comparison

In conclusion, two 0D models with and without beam extraction have been used to compare balance discharge characteristics. It has been shown that the discharge current and voltage should be different with and without extraction to balance the discharge. Finally the use of the 0D model with beam extraction with the output from the 0D model without extraction allows predicting at which electrical discharge parameter a discharge chamber tested without beam should be operate when the beam is extracted.

B. Experimental data comparison with 0D model without beam extraction

The 0D model without beam extraction is used to solve the balance of the configurations and operating conditions explored during the test campaign. The comparison between the 0D model and the experimental data allow tuning and validating the 0D model. The calibration of the 0D model with the experimental data allows using it as sizing tools with confidence.

The 0D model without extraction is compared with the experimental data presented in Table III-1. This database corresponds to 5 different magnetic fields (respectively from configuration 12 to 16) and different operating conditions used during the test campaign. The geometrical and magnetic parameters in the 0D model are adjusted to reflect each configuration. For each comparison, the 0D model uses as operating condition inputs the mass flow rate through the main feed line and the cathode, the discharge current, the simulated ion beam, and the cathode potential. It should be noted that $\widehat{Q_{in}}$ should include the gas back-ingestion due to the limited vacuum chamber pumping speed capability. In our case, the ingested gas is estimated at 10% of the income flow $Q_{ing} = \frac{1}{10} Q_{in}$.

Table III-1 – Experimental data used for comparison

Operating conditions				Experiment				
Configuration	Main MFR [SCCM]	HC MFR [SCCM]	Id [A]	Vd [V]	Screen grid [A]	Accel grid [A]	Residual beam [A]	Simulated Ib [A]
12	25	3.5	21	24.40	1.7	1.2	3.7E-03	2.17
12	25	4.5	21	23.24	1.5	1.1	3.7E-03	2.01
12	30	3.5	21	23.90	1.7	1.2	3.6E-03	2.17
12	25	3.5	23	23.33	1.6	1.1	4.0E-03	2.11
12	25	4.5	23	22.32	1.5	1.0	4.0E-03	1.98
12	30	3.5	23	23.02	1.6	1.1	3.9E-03	2.13
13	25	3.5	21	23.01	1.6	1.1	4.1E-03	2.08
13	25	3.5	23	22.72	1.7	1.2	4.8E-03	2.16
14	25	3.5	21	23.05	1.4	1.0	2.9E-03	1.89
14	25	3.5	23	23.39	1.5	1.1	3.3E-03	2.04
15	25	3.5	21	23.86	1.7	1.2	4.0E-03	2.21
15	25	4.5	21	22.47	1.6	1.1	4.1E-03	2.05
15	30	2	21	28.43	2.2	1.6	4.9E-03	2.75
15	30	3.5	21	23.31	1.7	1.2	4.0E-03	2.23
16	25	3.5	21	24.43	1.7	1.2	3.7E-03	2.18
16	30	3.5	21	24.03	1.7	1.2	3.4E-03	2.20
16	25	4.5	21	23.31	1.5	1.1	3.8E-03	2.03
16	30	2	22.5	29.24	2.3	1.6	3.9E-03	2.80

1. *0D model calibration, validation and deviation*

Until now, the cathode potential was fixed by default at V_c=10V, in fact, the cathode potential could vary as function of the operating conditions, coupling with discharge chamber and its own thermal properties. This value is used to tune the 0D model against the experimental data.

The data present in the table Table III-1 are fitted with the 0D model by solving the cathode potential V_c needed to match the corresponding experimental parameters. The averaged value found is about 10.7 V. In addition, in our data, the mass flow rate injected through the hollow cathode is between 2 and 4.5 SCCM. It is found that the requested cathode potential is higher when the mass flow rate in the hollow cathode is lower, which is the expected behavior of the potential in a cathode. Figure III-3 shows the cathode potential needed to fit the experimental data as a function of the cathode mass flow rate.

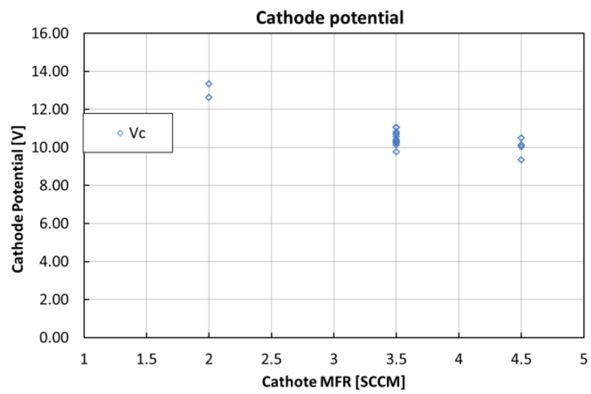

Figure III-3– Cathode potential needed to match experimental data & fitting curve

Finally, the 0D model with beam extraction is used to predict electrical discharge characteristics if the experiment is run with beam extraction. The 0D model uses the cathode potential found previously assuming that with beam extraction the flow rate through the cathode remains the same while only the main flow rate is increased. Figure III-4 plots on the left the discharge current with beam extraction as a function of the discharge current without beam extraction. It can be noted that with beam extraction the discharge current requested is lower than without beam extraction but still higher than the relation $I_D = \hat{I}_D - I_B$. On the right, the discharge voltage requested to sustain the discharge is plot as a function of the discharge voltage needed during the test campaign. It is shown that the requested voltage with beam extraction is lower than the one without extraction. In addition, the trend of the discharge voltage with versus without extraction is relatively linear, which means that the offset of discharge voltage without beam extraction can be estimated in approximatively -1.5 V.

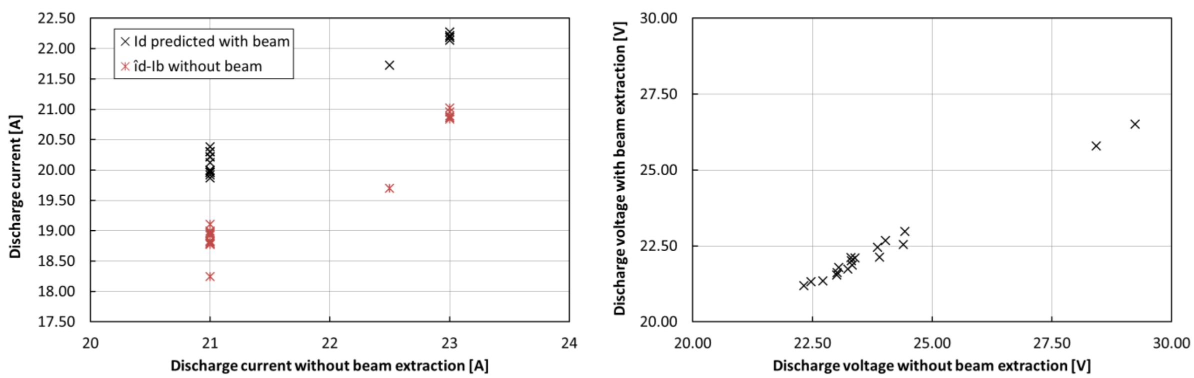

Figure III-4 – Electrics discharge characteristics without vs with beam extraction

IV. 2D model without beam extraction and validation

The 2D axisymmetric model originally developed with beam extraction [9] was largely based on work proposed by Wirz in this thesis [8]. It is a hybrid code which solves, at steady-state, the equilibrium between different species as primary electron, neutral, ion and secondary electron in the ring cusp discharge chamber. The code is called hybrid as the primary and neutral are solved with a PIC-MCC method, while the ion and secondary electron are solved with a fluid description by assuming magnetized ambipolar flux with a finite volume method solver. The flow chart of the 2D simulation is presented Figure IV-1. The discharge chamber model is executed by a main script, which initializes the simulation with parameters defined in a class object and then calls iteratively sub-model functions to bring the RCDC simulation to a steady-state converged solution, with mass, currents and energy conservation. The coupling between the sub-models for the different species is achieved through the collisions sub-model, mass conservation, and currents balance. To this purpose, the 2D model main loop consists of three sub-loops that are nested to iterate the solutions of the different sub-models until they converge towards the requested operating conditions.

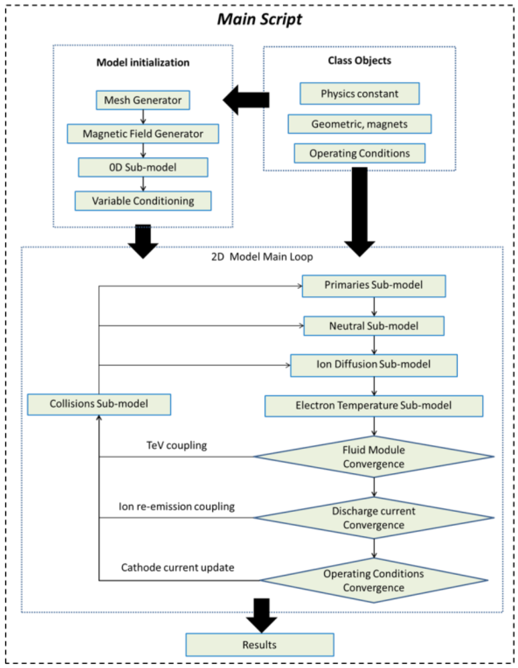

Figure IV-1 –Model flow chart

In order to compare the code with the experimental data, the original code is modified to simulate the RCDC operation without beam extraction. In addition to the electrical parameters, Langmuir probe measurements were taken during the test campaign, which allows comparing the simulated plasma properties distribution against the experimental data.

The following sections present the 2D axisymmetric model modifications needed to simulate the DC without beam extraction, a test case comparison of the simulated results with and without beam extraction and finally experimental and numerical results are compared with Langmuir probe measurements.

A. 2D model modifications for operation without beam extraction

With respect to the original code, few modifications were made to be allowing simulating the discharge chamber without beam extraction. The major modification is associated with the ion current collected by the ion optics and re-emitted as neutral in the DC. As described previously, the reduced ions transparency leads to high recombination of ions in the grid system.

The local neutral source at the grid from the recombination can be expressed as

$$\widehat{Q_{gd\_r}} = \widehat{\Gamma_\iota}\left(1 - \widehat{T_{dc}}\right) = \hat{n}\widehat{u_B}\left(1 - \widehat{T_{dc}}\right)$$

where $\widehat{Q_{gd\_r}}$ is the particle flow rate re-injected at the grid due to ion grid recombination and $\widehat{\Gamma_\iota}$ is the ion flux reaching the grid. The second modification was made on the current conservation equation, which, as it was previously described, can be written as

$$\widehat{I_a} = \widehat{I_e} + I_{tot} + \widehat{I_{\iota a}} - \widehat{I_L}$$

This equation is used to define the potential drop at the cusp required to balance the current in the discharge,

$$\widehat{I_a} = \frac{1}{4}\hat{n}\sqrt{\frac{q\widehat{T_{eV}}}{\pi m_e}}exp^{(-\phi/\widehat{T_{eV}})} \qquad \text{at the cusp}$$

B. Test case comparison of the 2D model with and without beam extraction

The 2D model is run with a test case which solve the discharge with and without beam extraction. After reaching the converged solutions, it was found that the discrepancy of the predicted ion flux reaching the grid is about 5%. Figure IV-2 shows the plasma radial density profile at the grid exit. In the case with beam extraction, the plasma density is higher than in the case without beam extraction, but the difference between both profiles is relatively small. This result builds confidence that the results of the 2D simulations without beam extraction can be used in a comparison with experimental data.

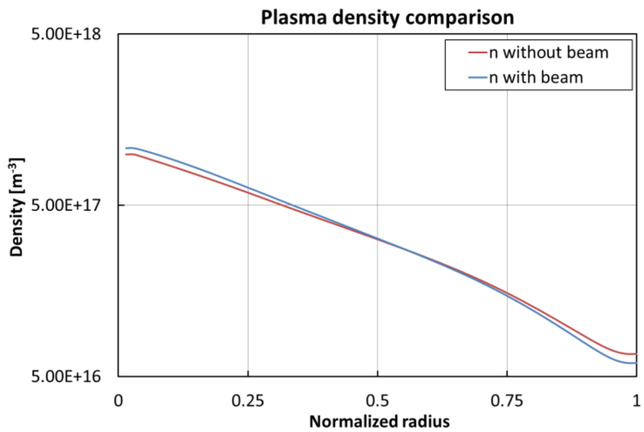

Figure IV-2-Ion flux at the grid exit - comparison with and without beam extraction

C. Experimental data comparison with 2D simulation

During the test campaign performed on the MSL prototype discharge chamber [10], Langmuir Probe (LP) measurements were taken inside the RCDC close to the grid extraction plane. The probe was swept across the grid diameter to characterize the profile of the plasma properties, in particular, the plasma density. Figure IV-3 shows the LP during a measurement sweep inside the prototype ring cusp thruster operating in discharge mode in the MSL laboratory.

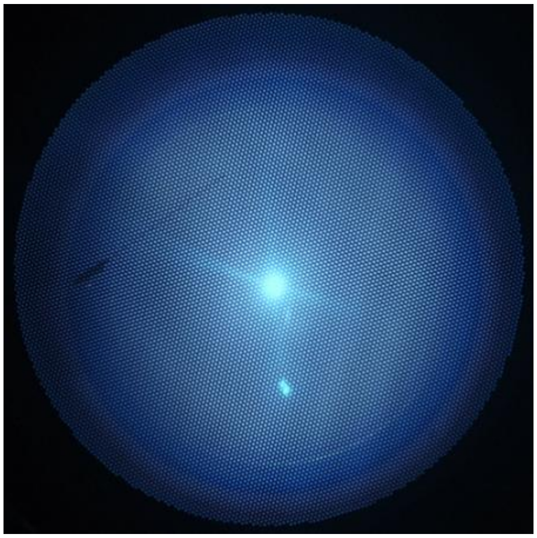

Figure IV-3- Langmuir probe in the DC

The data acquired with the LP has been post-processed using the Druyvesten technique [11], which extracts information regarding the plasma density, electron temperature and plasma potential from the probe *I-V* curve characteristics. In addition, the EEDF is fitted with a Maxwellian distribution function in order to correct, in first approximation, the magnetic field effect on the effective current collected on the probe [12]. By integrating the plasma properties across the exit plane, it is possible to evaluate the ion as flux reaching the grid as

$$I_{tot} = 2\pi q \int n(r)u_B(r)rdr$$

The data selected for the comparison are presented on Table IV-1. The data chosen to run the simulation correspond to experimental data that shown low relative error between measured current on the grid and integrated flux with the LP which corresponds to three cases and three different magnetic field configurations.

Table IV-1-Comparison between Electrical characteristics and LP measurement

Configuration	Main MFR [SCCM]	HC MFR [SCCM]	Idc [A]	Vd [V]	Itot [A]	Trans	Ib [A]	I LP exp [A]	Beam Flatness Ratio exp	exp relative error
12	30	3.5	23	23.01	2.68	0.79	2.13	2.65	1.86	1%
13	25	3.5	23	22.74	2.73	0.79	2.16	2.71	2.78	1%
15	30	2	21	28.44	3.69	0.75	2.75	3.64	2.27	1%

The magnetic field of the configuration 12, 13 and 15 are shown Figure IV-4, few modifications are present between these, in particular on the top at the grid exit would allow to a modification of the plasma properties profile. The black area in the picture represent the discharge cathode, the primary injection in the discharge chamber is at the same place for configuration 12 and 13 and forward in with configuration 15.

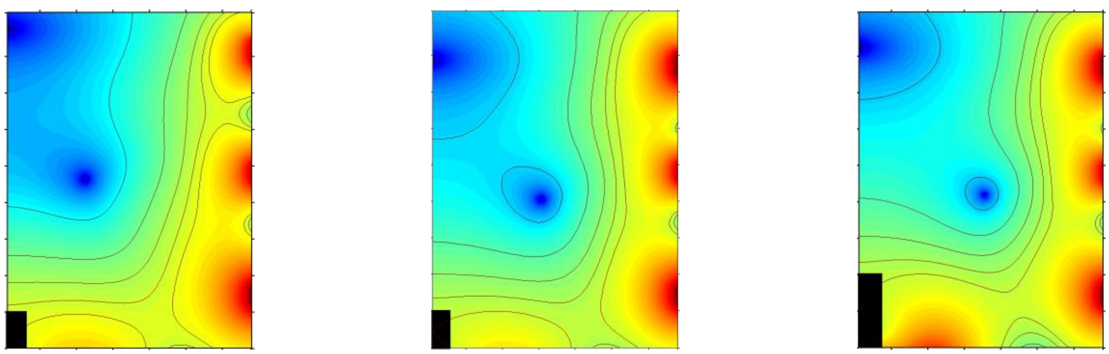

Configuration 12 *Configuration 13* *Configuration 15*

Figure IV-4 – Magnetic field topologies

The 2D axisymmetric model is used to simulate each configuration and operating conditions to evaluate the ability of the model to reproduce the experimental results. From each simulation, the distributions of the primaries, neutral, plasma density and electron temperature are presented. The converged results are obtained with approximatively 20 main iterations on the injected primary current to reach the requested operating conditions (discharge voltage and current, at given mass flow rates).

1. Primary density

Figure IV-5 shows primaries densities for each simulated configuration. The primaries are injected from the cathode and are distributed in the magnetized DC by following the magnetic lines. It can be shown in function of the magnetic field topologies; the distributions of the primaries are different. Optimized magnetic field topologies should allow enhancing the deposited power in the DC and then the ionization process. In the cases of the configuration 12 with the biggest area at low magnetic field in the middle, it is shown that the primaries are more attracted by the different cusps in the DC and are spatially more distributed in the DC than the configuration 13 and 15.

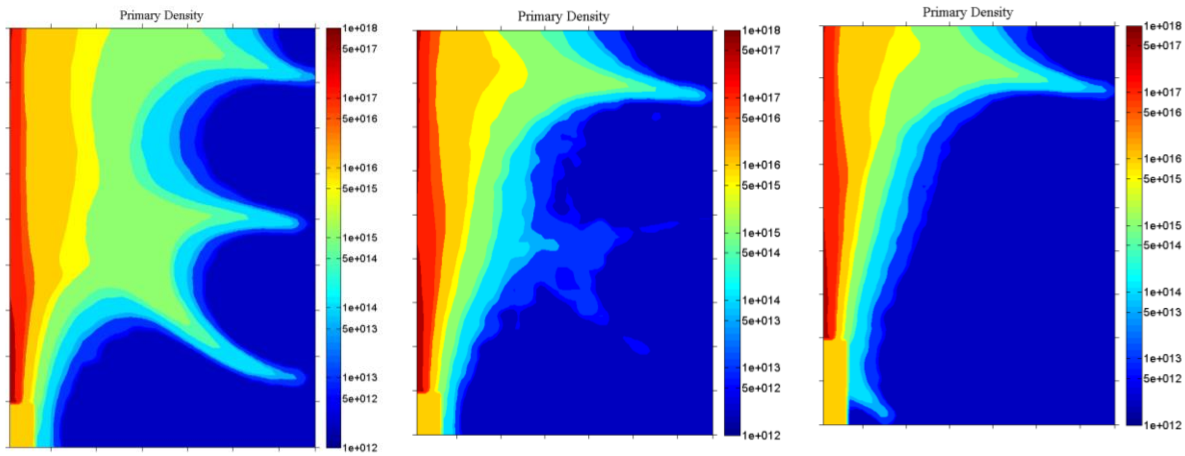

Configuration 12 | Configuration 13 | Configuration 15

Figure IV-5 – Primaries densities

2. Neutral density

Figure IV-6 neutral densities for each simulated configuration. On the axis most of the neutral are depleted due to the presence of ionization due by the primaries electron coming from the cathode. On the bottom, the highest density is due to the main gas injection location and on the walls where the ions flux is re-emitted as neutral. No significate difference is shown between the different simulated conditions, on configuration 12, the highest depleted area is bigger than other conditions due to the more distributed primary.

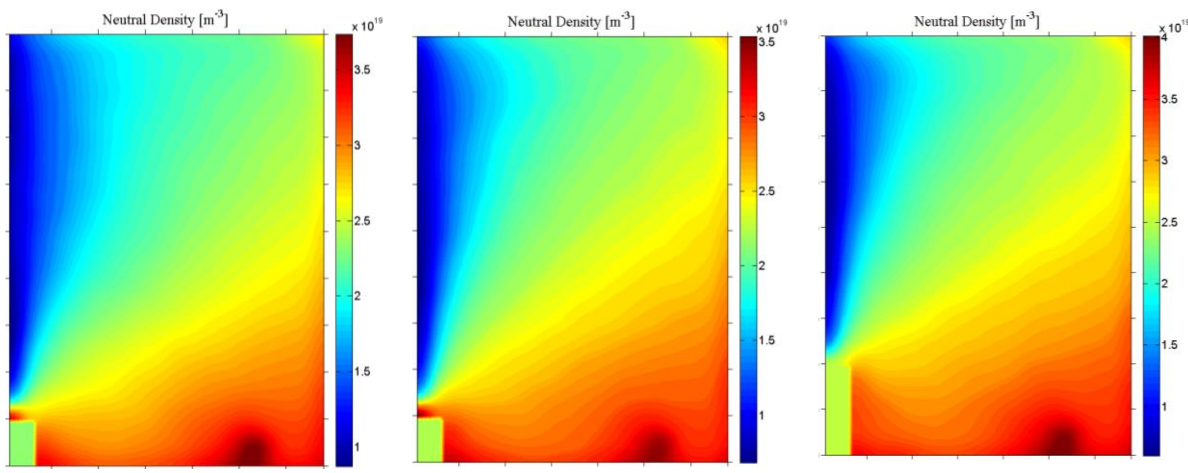

Configuration 12 | Configuration 13 | Configuration 15

Figure IV-6 Neutral densities

3. Plasma density

Figure IV-7 shows plasma densities for each simulated configuration. It can be shown that the bulk plasma is generated at the exit of the cathode where energy is injected through the primaries to ionize the neural and create ion plasma. Here the plasma density is solved by using magnetized ambipolar diffusion [7] [13]. The plasma density is sensitive to the magnetic field, while the density is lower between cusps on the boundary, which is basically the expected plasma confinement to the anode wall.

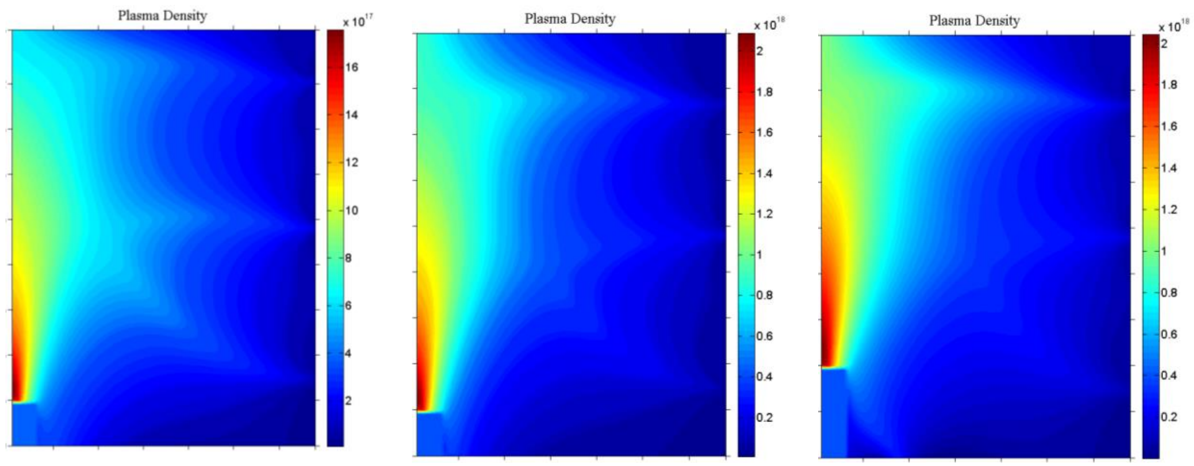

Configuration 12 *Configuration 13* *Configuration 15*

Figure IV-7 Plasma densities

4. Electron temperature

Figure IV-8 shows electron temperatures for each simulated configuration. It can be shown that to balance the energy in the discharge chamber, the electron is the highest at the cathode exit and the lowest on the anode wall boundary. The low electron temperature and plasma density at the walls allow a weak ion current flux to the wall and better discharge efficiency to produce the beam.

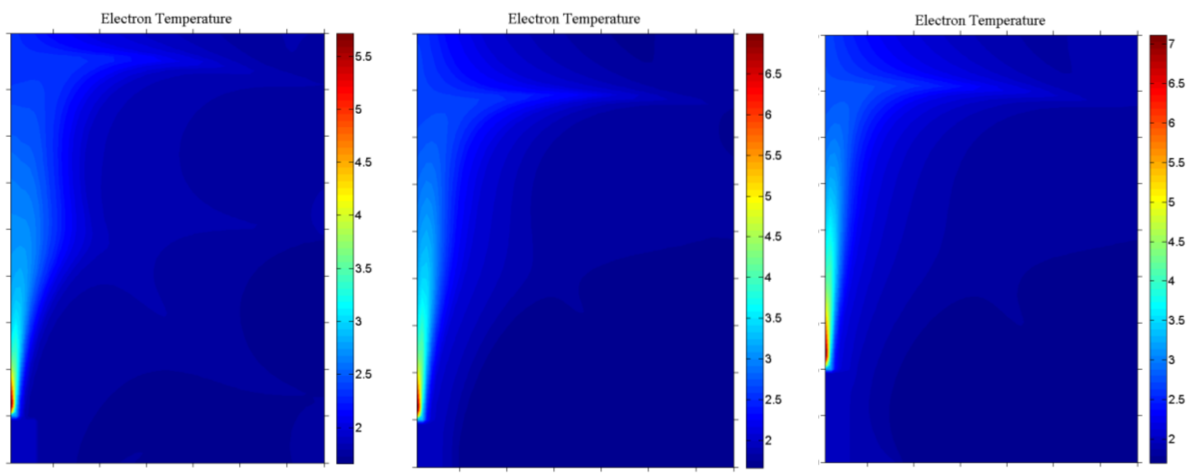

Configuration 12 *Configuration 13* *Configuration 15*

Figure IV-8 Electron temperature

5. Comparison with Langmuir probe measurement

Figure IV-9 shows the comparison of the simulated plasma density profile at the grid extraction plane and the Langmuir probes measurements. For each configuration, it can be shown that, in respect of the estimation of the plasma properties used for the LP and the 2D model assumptions, the magnitude order of plasma density is simulated but the plasma density is overestimated on the middle and underestimated on the edge. From a quantitative point of view, the simulation conditions 12-13-15 predict an ion flux reaching the grid of respectively 3.10 A, 3.18 A and 4.11 A which is 16%, 17% and 12% above the experimental result, which give an average offset deviation about 15%. For what concerning the simulated beam, the offset deviation of the simulation is estimated at 7%, the different deviation between the ion flux at the grid and the simulated ion beam is due to the presence of the masking area on the edge of the grid.

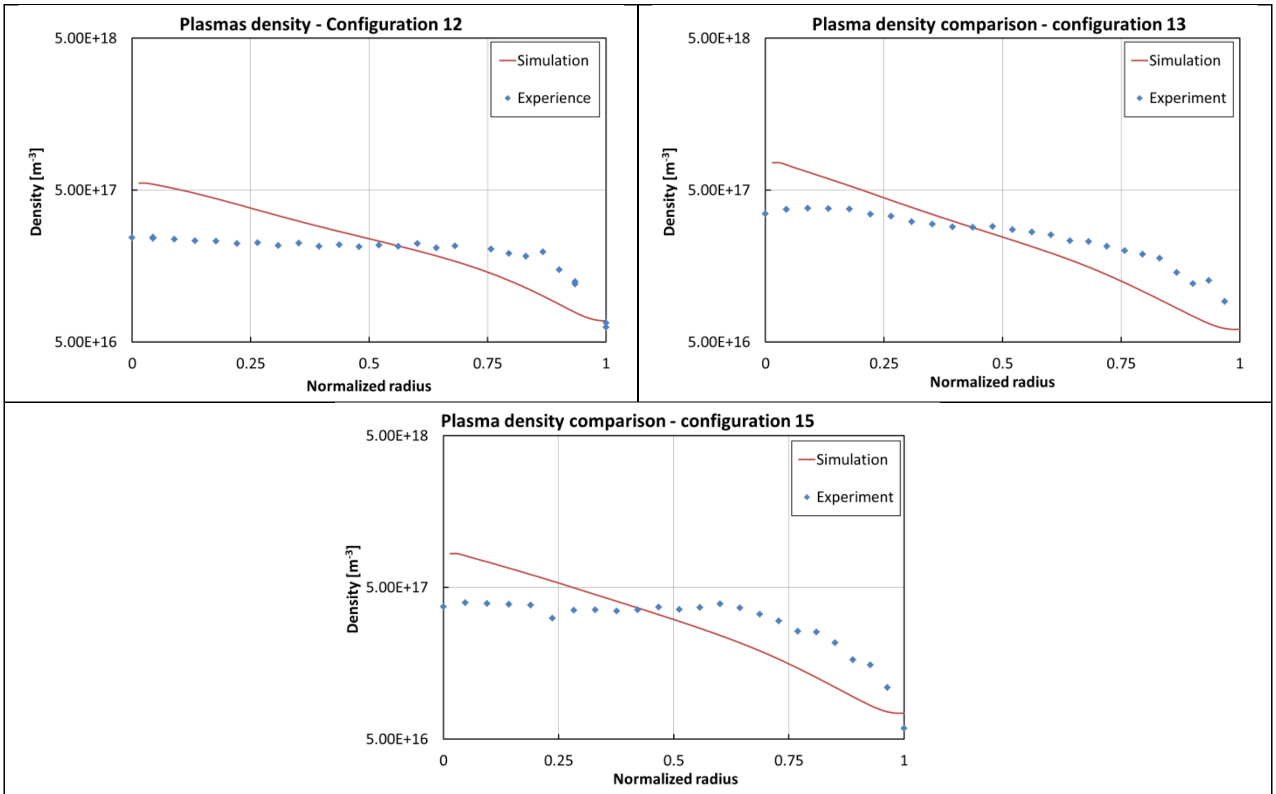

Figure IV-9- Plasma density close to the grid extraction plane

6. *Discussion*

The differences between model and experimental data can be explained with several reasons. From the plasma diffusion point of view, the use of uniform and structured mesh is susceptible to numerical diffusion due to the non-alignment with the magnetic field. It has been shown that using a magnetic field aligned mesh can provide superior accuracy, especially in the bulk plasma and near-cusp regions [14]. A second reason which can explain this difference is the used assumptions of the Maxwellian electron distribution function for secondaries and then ambipolar coefficient definition. In reality, in low-temperature plasma, electron distribution is unlikely Maxwellian [15], due to first the presence of fast and slow electron and Coulomb interactions. In addition, the magnetized diffusion is defined for quasi-neutral plasma, while in our case the production rate of electron is higher than ions (which allow solving the discharge current at the anode) and the double ion production is not taken into account. Finally, the electron transport and ambipolar diffusion is still subject to numerous studies to compare theoretical assumptions and numerical results, as such anomalous transport in drift transport. It as being recently shown that using an axisymmetric full PIC model [16] to simulate the plasma inside the ring cusp discharge chamber allows dealing with the time-varying electromagnetic which have a great influence on the evolution of the plasma, ions and electron transport, which can potentially overcome the Maxwellian description used with fluid description.

V. Conclusion

Analytical and numerical simulation tools to design and interpret ring cusp discharge chamber measurement have been developed in MSL. The tools have been compared derivate from the literature in order to represent the experiment campaign realized without beam extraction. The 0D model and 2D axisymmetric have been compared and again the experimental data and a tuned procedure have been realized to fit the experiment with a predicted deviation error. The 2D axisymmetric simulation which solves physics assumptions have been compared with experimental data from the LP, the value is founded in the respect of the magnitude order but some deviation on the exit profile is appearing, some explanation of the deviations are proposed in order explained the behaviour and giving considerations to improve accuracy of the code for further development in the future.

VI. References

[1] F. Cannat, F. Guarducci, S. Ciaralli, M. Coletti and S. Gabriel, “Design and optimization of a Ring Cusp thruster with simulated beam extraction,” in *IEPC*, Atlanta, 2017.

[2] F. Cannat, F. Guarducci, S. Ciaralli and S. Gabriel, “Design and performance characterization with simulated ion beam extraction,” in *Space Propulsion 2018*, Seville, 2018.

[3] J. R. Brophy, “Simulated ion thruster operation without beam extraction,” in *21st International Electrical Propulsion Conference*, 1990.

[4] N. A. Arthur and J. E. Foster, “Characterization of a cylindrical ring-cusp ion source with electrically isolated magnet rings,” *Journal of Vacuum Science & Technology A: Vacuum, surfaces and films*, p. 021210, 2017.

[5] B. Dankongkakul and R. E. Wirz, “Design of Miniature Ring-Cusp Ion thrusters via analysis of discharge EEDF and plasma parameter mapping,” in *52nd Joint Propulsion Conference*, Salt Lake City, 2016.

[6] J. E. Foster, A. Hubble, S. Nowak-Gucker, C. Davis, P. Peterson, E. Viges and D. Chen, “Simulated Beam extraction performances characterization of a 50-cm Ion thruster Discharge,” in *48th Joint propulsion conference*, Atlanta, 2012.

[7] D. M. Goebel and I. Katz, Fundamentals of Electric Propulsion: Ion and Hall Thrusters, JPL, California Institute of Technology: JPL Space Science and Technology Series, 2008.

[8] R. Wirz, “Discharge Plasma Processes of Ring-Cusp Ion Thrusters,” Thesis, California Institute of Technology, Pasadena, California, 2005.

[9] F. Cannat, F. Guarducci, S. Ciaralli and S. Gabriel, “2D axisymmetric numerical model development and validation,” in *Space Propulsion 2018*, Seville, 2018.

[10] F. Cannat, F. Guarducci, S. Ciarralia and S. Gabriel, “Design and performance characterization with simulated ion beam extraction,” in *Space Propulsion 2018*, Seville, 2018.

[11] V. A. Godyak and V. I. Demidov, “Probe measurements of the electron energy distributions in plasma,” *Journal Physics Appl Phys* , vol. 44, no. 233001, p. 20, 2011.

[12] T. K. Popov, P. Ivanova, M. Dimitrova, J. Kovacic, T. Gyergyek and M. Cercek, “Langmuir probe measurement of the eletron distribution function in magnetized gas discharge plasma,” *Plasma Sources Sciences and Technologies*, p. 025004, 2012.

[13] M. A. Lieberman and A. J. Lichtenberg, Principles of Plasma discharges and materials processing, John Wiley & Sons, 2005.

[14] S. J. Araki and R. E. Wirz, “Magnetic Field Aligned Mesh for Ring-Cusp Discharge Chamber,” in *50th Joint Propulsion conference*, Cleveland, 2014.

[15] V. Kolobov and V. Godyak, “Electron kinetics in low-temperature plasmas,” *Physics of Plasmas*, vol. 26, p. 060601, 2019.

[16] S. L. Guo, X. L. Jin, L. Lei, X. Y. Zhang, X. F. Zhu, Z. H. Yang and B. Li, “Numerical simulation of plasma and electromagnetic characteristics for an ion thruster discharge chamber,” *Physics of Plasmas*, vol. 26, p. 073502, 2019.